Nanoscale

PAPER

View Article Online
View Journal | View Issue

Cite this: *Nanoscale*, 2022, **14**, 14683

Anti-aggregation effect of carbon quantum dots on diabetogenic and beta-cell cytotoxic amylin and beta amyloid heterocomplexes

Anna Voronova, Alexandre Barras, Valérie Plaisance, Valerie Pawlowski, Rabah Boukherroub, Amar Abderrahmani* and Sabine Szunerits *

Pancreatic islet amyloid deposition is a pathological hallmark of Type 2 diabetes (T2D), contributing to reduced functional β-cell mass. Islet amyloids result not only from the aggregation and fibrillation of human islet amyloid polypeptide (hIAPP), but also from beta-amyloid 42 (Aβ42), the key amyloidogenic peptide linked to Alzheimer's disease. Importantly, Aβ42 and hIAPP aggregates (IAPP:Aβ42) can interact with each other and form some harmful heterocomplex fibrils. While it is well-documented that hIAPP aggregation occurs only when islets are exposed to a diabetic environment, including hyperglycemia and/or elevated concentrations of saturated fatty acids (SFAs), it remains unclear if hIAPP and IAPP:Aβ42 heteromer fibrillations are directly or indirectly triggered by this environment. In this study, we show the interplay between high glucose concentrations and palmitate as the SFA in the aggregation of hIAPP. In addition, we outline that the interaction of hIAPP and Aβ42 leads to the formation of complex protein aggregates, which are toxic to β-cells. Carbon nanocolloids in the form of positively charged carbon quantum dots (CQD-pos) efficiently prevent single amyloid aggregation and the formation of IAPP:Aβ42 heterocomplexes. We provide clear evidence with this study that the diabetogenic environment of islets could directly contribute to the formation of homomeric and heteromeric amyloid aggregates and fibrils in T2D. We also propose carbon nanocolloids as biocompatible nanomaterials for developing innovative therapeutic strategies that prevent the decline of functional β-cell mass.

Received 8th June 2022,
Accepted 7th September 2022

DOI: 10.1039/d2nr03173f

rsc.li/nanoscale

1. Introduction

Type 2 diabetes (T2D) is one of the deadliest chronic diseases worldwide. The disease develops when β-cells from pancreatic islets fail to produce an adequate level of insulin for the body's needs. In T2D, β-cell failure results from cell dysfunction and the progressive decline of β-cell mass mainly caused by cell death. Numerous observational and preclinical studies have confirmed the key role of islet amyloid deposits in β-cell loss in the pathophysiology of T2D.[1–3] In humans, islet amyloid deposits are mainly formed by the oligomerization, aggregation and fibrillation of islet amyloid polypeptide (hIAPP), also called amylin, a hormone co-expressed and co-secreted with insulin by pancreatic β-cells. Although hIAPP aggregation occurs only when islets are exposed to a diabetic environment, including hyperglycemia and/or elevated concentration in saturated fatty acids (SFAs),[4] it is still unclear if hIAPP oligomerization and fibrillation are directly or indirectly triggered by this environment. In addition, there are several bodies of evidence stating that islet amyloid could result from the association of hIAPP fibrils with beta-amyloid 42 (Aβ42) aggregates, one of the main oligomer species that is responsible for amyloid plaque and neuronal loss in Alzheimer's disease.[5]

Indeed, islet β-cells express the amyloid precursor protein (APP) and the enzymatic machinery generates the amyloidogenic Aβ42.[6–9] In addition, Aβ42 interaction with hIAPP[10] has been detected in pancreas from patients and animal models of T2D.[9,11–13] Some studies have revealed that the heteromeric oligomer structure (heterocomplex) formed by hIAPP and Aβ42 could be more cytotoxic than the single oligomers.[10] While this hypothesis was validated in a neuronal cell model, it remains unclear for β-cells exposed to diabetogenic factors. If so, for an antidiabetic strategy triggering the islet amyloid, it is key to search for molecules that inhibit the formation of hIAPP:Aβ42 heterocomplexes and/or redirect the aggregation cascade towards off-pathway species with reduced toxicity. Such molecules could represent an innovative antidiabetic class that prevents and/or reduce β-cell loss in T2D. This is possible as exemplified by the discovery of several molecules inhibiting the single aggregation of soluble Aβ monomers or hIAPP.

Univ. Lille, CNRS, Centrale Lille Univ. Polytechnique Hauts-de-France, UMR 8520 – IEMN, F-59000 Lille, France. E-mail: sabine.szunerits@univ-lille.fr, amar.abderrahmani@univ-lille.fr

The development of biocompatible nanomaterials with the ability to interfere with protein fibrillation has been considered as a promising alternative to chemical- and biological-based inhibitors.[14–16] For example, chaperon gold nanoparticles were employed to eliminate the toxicity of Aβ42 in a zebrafish model.[17] Carbon quantum dots (CQDs) are an emerging subset of nanomaterials, defined by characteristic sizes of <10 nm and a carbon core that is functionalized by various groups at the surface. CQDs have been reported as potent inhibitors against the *in vivo* aggregation and toxicity of hIAPP.[18,19] In addition, the group of Leblanc showed that amphiphilic CQDs were effective in inhibiting the overexpression of APP and Aβ42.[20] CQDs also prevented IAPP fibril formation in response to lipopolysaccharides. The inhibitory effect of CQDs was ascribed to their hydrophobic and π–π stacking interactions with amyloid peptides. Numerical computational studies of tetramer and octamer hIAPP with or without diverse carbon nanoparticles, such as graphene, single-walled carbon nanotubes (SWCNTs) and fullerene C_{60}, revealed that peptides can be strongly adsorbed onto graphene and SWCNTs, while C_{60} prevents aggregation to a lesser extent.[2]

The goal of the study was to investigate the ability of differently-functionalized CQDs to inhibit the aggregation of hIAPP and Aβ42 homomeric fibrils as well as hIAPP:Aβ42 heteromeric fibril complexes in *in vitro* and *ex vivo* β-cell models exposed to diabetogenic factors. The novelty of the study is, on one hand, the demonstration of the possible interaction of hIAPP and Aβ42 under simulated type 2 diabetes (T2D) conditions, showing the influence of glucose and fatty acids on INS-1 cell toxicity and rat islets. Furthermore, the potential of CQDs as an anti-aggregation agent working efficiently under diabetic conditions is underlined. We show that the T2D diabetic conditions do not alter the functionality of the nanoparticles, which maintain their effectiveness in *in vitro* and *ex vivo* experiments.

2. Results and discussion

2.1. Human islet amyloid polypeptide (hIAPP) aggregation and fibrillation in response to direct exposure to glucose and saturated fatty acids

Initially, we wanted to determine if high glucose and/or saturated fatty acid (SFA) concentrations directly induce hIAPP fibril formation. For this reason, we monitored hIAPP aggregation by thioflavin-T (ThT) in the presence of low glucose (5 mM), high glucose (33 mM) and different concentrations of palmitate as SFA over a time span of 12 h. Fig. 1a displays the typical sigmoidal growth curves of hIAPP (20 μM) aggregation with a lag phase of about 1.5 h where no hIAAP fibrils are evident. The use of 20 μM hIAPP, even though higher than the physiological concentration level, has been established as the optimal concentration for homodimer and heterodimer aggregations.[10,21] During the elongation phase, monomers undergo conformational rearrangement, leading to the formation of clusters that induce fibrillation and increase ThT fluorescence. This step is considered as a critical and rate limiting step. Equilibrium is reached after about 6 h, as seen in the saturation of the fluorescence intensity change. The atomic force microscopy (AFM) image in Fig. 1b corroborates

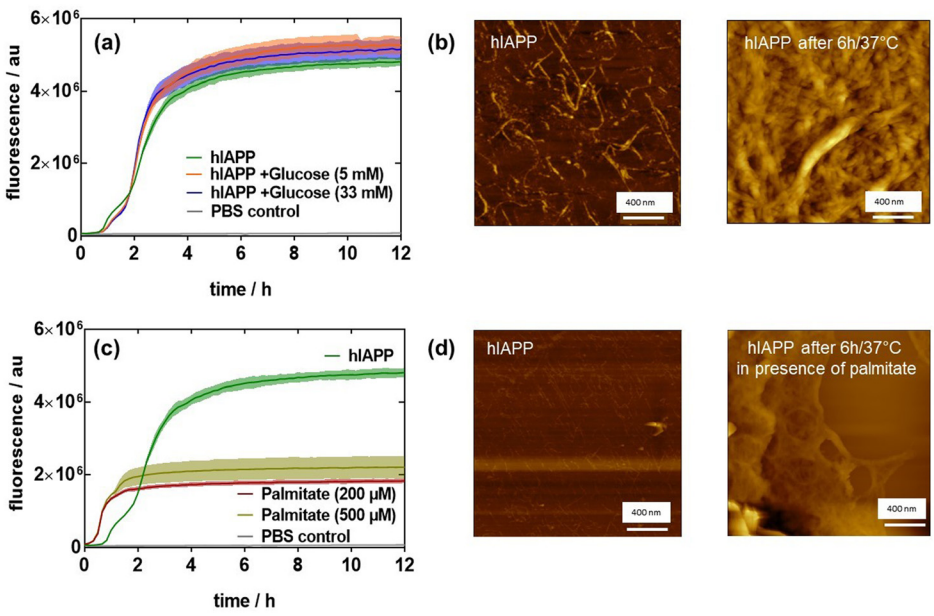

Fig. 1 Effect of glucose (5–33 mM) and palmitate (200–500 μM) on the fibrillation of hIAPP: (a) Thioflavin-T fluorescence intensity as a function of glucose concentration (5 and 33 mM) on hIAPP (20 μM) aggregation at 37 °C. (b) AFM images of hIAPP (20 μM) before and after aggregation for 6 h at 37 °C. (c) Thioflavin-T fluorescence intensity as a function of palmitate concentration (200 and 500 μM) on hIAPP (20 μM) aggregation at 37 °C. (d) AFM images of hIAPP (20 μM) before and after aggregation for 6 h at 37 °C in the presence of 200 μM palmitate. The results are expressed as the mean ± SEM of at least 3 independent samples for each group.

the fluorescence results and indicates the presence of aggregated hIAPP after 6 h. To investigate the potential effect of glucose on hIAPP aggregation, 20 μM hIAPP was incubated with 5 or 33 mM glucose at 37 °C under physiological conditions[22] on the basis that healthy people have a glucose level of around 5 mM, which is increased up to 33 mM for diabetic patients. The presence of increased glucose levels had a minimal effect on hIAPP aggregation, with an increase of ThT fluorescence for 33 mM glucose (Fig. 1a).

It was previously reported that lipids can induce high amylin expression.[23] The influence of free fatty acids on hIAPP aggregation was thus monitored. For that, 20 μM hIAPP was incubated without and with sodium palmitate (200 or 500 μM). The results in Fig. 1c infer that palmitate accelerates hIAPP fibrillation with an increase in fluorescence after a lag time of 30 min but then levels off after 2 h. As reported by Mo *et al.*,[24] hIAPP exhibited a longer lag time compared with palmitate-treated hIAPP, indicating that palmitate accelerates the formation of hIAPP fibrils. However, palmitate-treated hIAPP resulted in a lower fluorescence level compared to hIAPP in the absence of palmitate, and only a few linear fibrils together with significant amounts of amorphous aggregates were observed in palmitate-treated hIAPP (Fig. 1d), while the AFM image of hIAPP after 6 h revealed a mesh of typical long linear fibrils (Fig. 1b).

2.2. Heteromeric amyloid complex formation by Aβ42 and hIAPP

Next, we assessed the aggregation behavior of hIAPP in the presence of low and equal concentrations of β-amyloid Aβ42 (Fig. 2). Unlike hIAPP, Aβ42 at a concentration of 20 μM did not feature any aggregation over a time span of 24 h (Fig. 2a). The addition of a small amount of hIAPP (2 μM, 10%) to Aβ42 shows fluorescence at the starting point, indicating that some heterooligomers might have been already formed (Fig. 2b). However, there is only a slight increase in fluorescence after 20 h, remaining much lower than that of hIAPP alone. At an equal concentration ratio of hIAPP and Aβ42 (20 : 20 μM), significant fibrillation occurs after a lag time of 14 h, approaching the fluorescence level of hIAPP alone. The addition of glucose to hIAPP:Aβ42 (1 : 1) at 20 μM strongly accelerates the fibrillation of the protein aggregates. However, the presence of palmitate as well as the combination of palmitate and glucose led to a lower fibrillated fiber content. These results clearly indicate that the interplay between hIAPP, Aβ42, palmitate and glucose is a complex process. To confirm the changes observed in the aggregation profile of Aβ42 co-incubated with hIAPP, denaturing immunoblotting using antibodies against Aβ42 was performed to detect the formation of aggregates (Fig. 2c). 20 μM hIAPP:Aβ42 (1 : 1) mixtures were left overnight at 4 °C

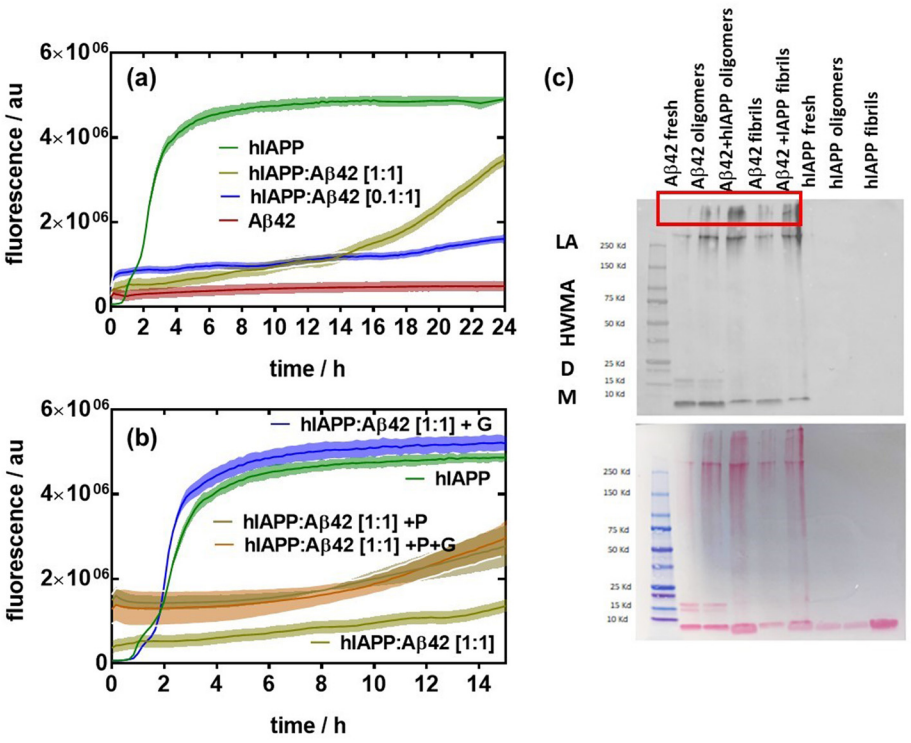

Fig. 2 Effect of Aβ42 on the fibrillation of hIAPP: (a) Thioflavin-T fluorescence intensity as a function of time of hIAPP (20 μM), Aβ42 (20 μM) and two ratios of hIAPP:Aβ42. (b) Thioflavin-T fluorescence intensity as a function of time of hIAPP (20 μM), hIAPP:Aβ42 (1/1 (20 μM) in the presence of glucose (33 mM) (blue), palmitate (grey) and glucose and palmitate together (brown). (c) Western immunoblotting analysis of the heterocomplexes of hIAPP:Aβ42 (1 : 1). Oligomers were formed after incubation for 24 h at 4 °C while fibrils were obtained after incubation for 24 h at 37 °C. The results are expressed as the mean ± SEM of at least 3 independent samples for each group.

and 37 °C to form oligomers and fibrils, respectively. The oligomerization and fibrillation of Aβ42 alone were compared to a freshly prepared Aβ42 solution. All samples demonstrated the ability to form large aggregates (>250 kDa). Moreover, hIAPP:Aβ42 oligomers and fibrils produced larger aggregates.

2.3. Cytotoxicity of hIAPP, Aβ42 and hIAPP:Aβ42 mixtures in the presence of glucose and palmitate to INS-1 cells

To test the cytotoxicity of the aggregates, rat insulinoma (INS-1) cells were incubated with hIAPP, Aβ42 and hIAPP:Aβ42 heterocomplexes in a medium containing 11 mM glucose and 0.5 mM palmitate (lipotoxic conditions) (Fig. 3a). BSA was used as a control because palmitate was coupled to this. In fact, we have added 0.1% (vol/vol) of BSA in the medium. As shown by previous studies,[25,26] our experiments confirmed that BSA did not affect the cell viability at 11 or 5 mM glucose. Then, we compared the toxicity of aggregates on cells cultured in the medium containing 11 mM glucose or 5 mM glucose (control medium) with either BSA or palmitate (Fig. 3b). In the medium containing 11 mM glucose and BSA, only oligomerized Aβ42 and the hIAPP:Aβ42 heterocomplex significantly affected the viability of INS-1 cells when compared to the control medium (Fig. 3a). The toxic effect of the hIAPP:Aβ42 heterocomplex is mainly due to oligomerized Aβ42. Indeed, hIAPP alone had no toxic effects at 11 mM and 5 mM. Interestingly, the toxic effect of oligomerized Aβ42 did not appear with 5 mM glucose. Cytotoxicity induced by oligomerized Aβ42 with 11 mM glucose was further amplified by palmitate. The presence of palmitate next to glucose promoted cell toxicity in all cases by a mechanism that is independent of cell function.[23] Our result confirms that amyloid generation and toxicity could only occur under diabetogenic conditions including high glucose concentration and SFA. The hIAPP:Aβ42 heterocomplex was clearly found to be more cytotoxic than the single oligomers and/or aggregates of hIAPP in INS-1 rat cells. In the cytotoxicity caused by the heterocomplex, our findings unveil the critical role of the Aβ42 oligomers/aggregates. In the presence of high glucose concentration and palmitate, the Aβ42 oligomers/aggregates *per se* are sufficient for reducing the cell viability. These results support the hypothesis that Aβ42 oligomers/aggregates are critical components of the amyloid deposits found in the islets of patients with T2D, which form a harmful heteromeric complex with hIAPP in pancreatic β-cells exposed to chronic hyperglycemia and SFA.

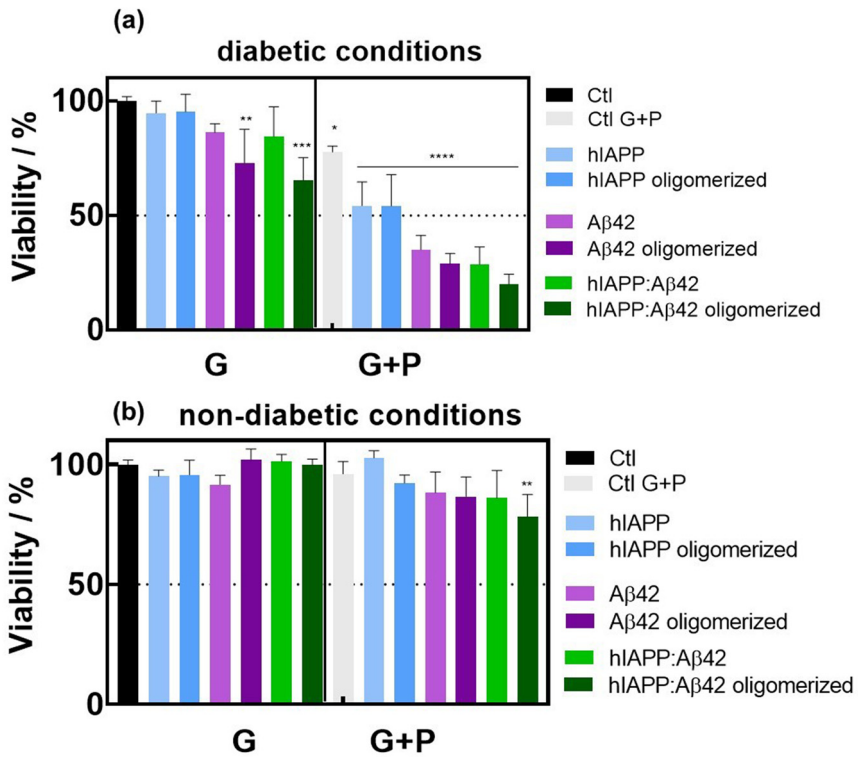

Fig. 3 Cytotoxicity studies in INS-1 cells: (a) viability of rat INS-1 cells cultured in a medium containing 0.1% (vol/vol) of BSA and 11 mM glucose (G) or 11 mM glucose and 0.5 mM palmitate (G + P), in the absence (Ctl) or presence of either fresh (non-oligomerized) or aggregated (6 h, 37 °C) hIAPP (20 μM), Aβ42 (20 μM) and hIAPP:Aβ42 mixtures. (b) Viability of INS-1 cells cultured with or without the aggregates in a medium (supplemented with 0.1% (vol/vol) of BSA) containing 5 mM glucose (G) or 5 mM glucose and 0.5 mM palmitate (G + P) as described above. INS-1 cells were cultured in RPMI-1640 medium supplemented with 10% fetal bovine serum (FBS), 1% penicillin–streptomycin, 1% sodium pyruvate, and 50 μM β-mercaptoethanol seeded at a density of 10^5 cells per well in a 96-well plate and grown for 24 h before the assay. The cell viability was evaluated using the resazurin cell viability assay. The results are expressed as the mean ± SEM of at least 3 independent samples for each group. *$p < 0.05$; **$p < 0.01$; ***$p < 0.001$; and ****$p < 0.0001$, one-way ANOVA test against control (black); the difference between Aβ42 and Aβ42 oligomerized and hIAPP:Aβ42 and hIAPP:Aβ42 oligomerized is n.s.

2.4. Inhibitory effect of carbon quantum dots on hIAPP and Aβ42 aggregation processes

Protein aggregation has been reported to be inhibited by carbon nanomaterials such as graphene and carbon quantum dots (CQDs). These particles initiate contact with hIAPP through electrostatic and hydrophobic interactions as well as hydrogen bonding, resulting in the inhibition of peptide fibrillization.[18] Studies by Yousaf *et al.*[19] and Koppel *et al.*[15] underlined further the importance of carbon-based quantum dots as inhibitors against hIAPP amyloid aggregation. In the presence of fluorine-functionalized graphene quantum dots (FCQDs), the morphology of hIAPP aggregates changed from entangled long fibers to short thin fibrils and amorphous aggregates.[19] The mitigation of hIAPP aggregation with 2.8 nm average diameter CQDs (prepared from coal as a carbon precursor) was demonstrated by Koppel *et al.*, showing a reduced β-sheet content in the presence of CQDs.[15] To better understand the influence of the surface composition of CQDs on the aggregation inhibition of hIAPP, three types of CDQs were prepared using the microwave-assisted hydrothermal method (Fig. 4a): (i) positively charged CQD-pos (ζ = +32.5 mV)[27] using glucosamine as a carbon precursor with ethylenediamine as a passivating agent (Fig. 4b), (ii) neutral CQD-neut *via* mixing glucose and hydrofluoric acid to catalyse the dehydration reaction,[19] (iii) negatively charged CQD-neg (ζ = −24 mV) using glucosamine as a precursor and β-alanine as a surface passivating agent. The particles were of spherical shape (Fig. 4c) with an average particle size of 16.8 nm (CQD-pos), 22.3 nm (CQD-neut) and 20.8 nm (CQD-neg).

The chemical composition of the three CQDs was assessed by X-ray photoelectron spectroscopy (XPS). The C_{1s} high resolution XPS spectra of the CQDs depict different carbon features (Fig. 5a–c). In the case of CQD-pos (Fig. 5a), the high-resolution plot of C_{1s} reveals the presence of five peaks corresponding to C=C (283.8 eV), C–C/C–H (285.0 eV), C–N/C–O (286.8 eV), C=O (287.9 eV) and O–C=O (289.2 eV). The presence of carbonyl and carboxylic functions is additionally validated by the presence of a band at 530.7 eV (C=O) in the O_{1s} high resolution spectrum, next to 531.5 eV (C–O). The N_{1s} high resolution spectrum can be curve-fitted with bands at 398.3 eV (pyridinic C=N–C), 399.1 eV (pyrrolic N–H) and 400.3 eV (graphite-like structure N–C_3). In the case of CQD-neut (Fig. 5b), the high-resolution spectrum of C_{1s} indicated the presence of four peaks due to C=C (284.2 eV), C–C/C–H (285.0 eV), –O–C=O (289.0 eV) and C–F (290.1 eV). The F_{1s} high resolution curve was fitted with a single band at 685.2 eV. For CQD-neg (Fig. 5c), the deconvoluted spectrum of C_{1s} comprises five components: C=C (283.8 eV), C–C/C–H (285.0 eV), C–N/C–O (286.2 eV), C=O (287.2 eV) and O–C=O (288.3 eV). The bands at 530.1 eV (C=O) and 531.6 eV (C–O) in the O_{1s} high resolution spectrum imply the presence of oxygen functions. The N_{1s} high resolution spectrum shows comparable bands to those of CQD-pos: 398.3 eV (pyridinic C=N–C), 399.2 eV (pyrrolic N–H) and 400.9 eV (graphite-like structure N–C_3).

The chemical composition and the nature of the functional groups of the synthesized CQDs were further investigated by Fourier-transform infrared (FT-IR) spectroscopy (Fig. 6a). The FTIR spectrum of CQD-pos contains a broad band (3410–3420 cm^{-1}) attributed to the O–H/N–H stretching vibrations, whereas the C–H stretching and bending vibrations are located at 2932 and 1384 cm^{-1}, respectively. The band at 1636 cm^{-1} is due to the C=N and C=C bonds of the aromatic structure and the C=O stretching vibration (–NHCO–).

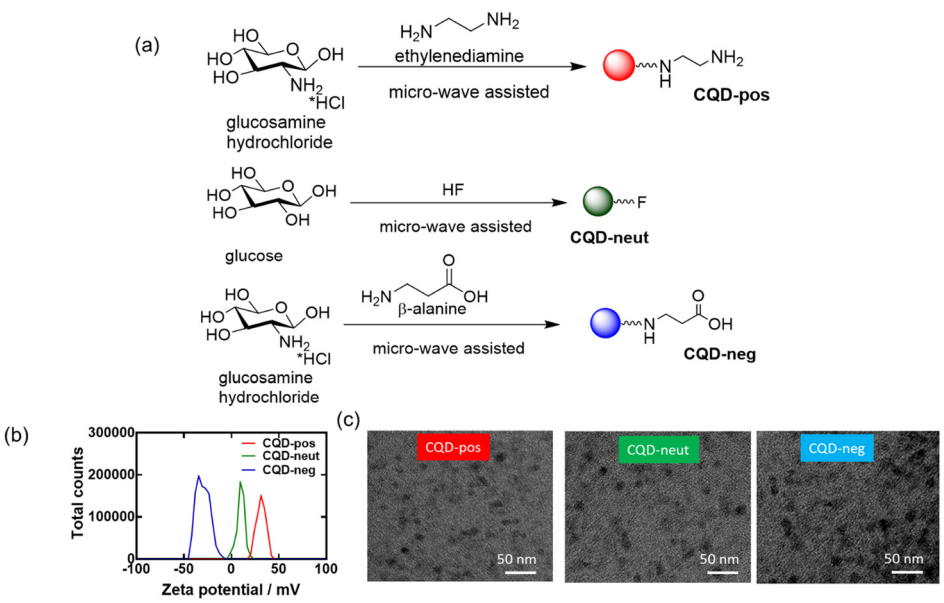

Fig. 4 Characterization of the CQD-pos, CQDs-neut and CQD-neg: (a) schematic representation of CQD synthesis. (b) Zeta potential analysis. (c) TEM images of the three nanostructures.

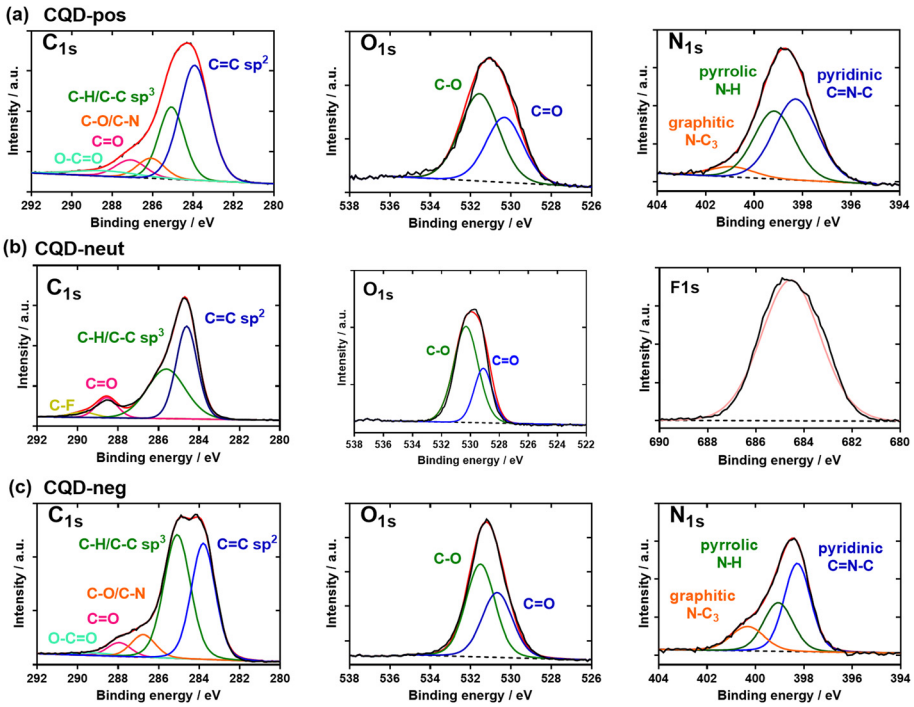

Fig. 5 Chemical composition of the three CQD types: XPS high-resolution spectra of the C_{1s}, O_{1s}, N_{1s}, and F_{1s} of (a) CQD-pos, (b) CQD-neut and (c) CQD-neg.

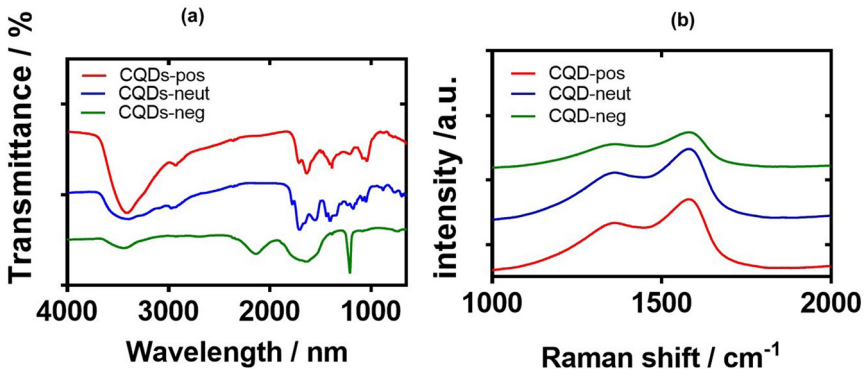

Fig. 6 FT-IR and Raman characterisations of CQDs: (a) FT-IR spectra of CQD-pos (red), CQD-neut (blue) and CQD-neg (green). (b) Raman spectra of CQD-pos (red), CQD-neut (blue) and CQD-neg (green).

Compared to CQD-pos, the more intense peaks at 1083 and 1041 cm^{-1} in the FTIR spectrum of CQD-neg are associated with the C–O stretching vibrations of either the residual carbohydrate or β-alanine. The sharp peak at 1710 cm^{-1} is assigned to the asymmetric stretching vibration of carboxylic acid moieties. In the case of CQD-neut, a sharp peak at 1100 cm^{-1} due to the stretching vibration of C–F suggests the doping of quantum dots with fluorine.[28]

Typical Raman spectra of the three CQDs are presented in Fig. 6b. The observed peaks are typical of sp^2 carbon materials at 1580 cm^{-1} (G-band) and 1378 cm^{-1} (D band), indicating that the materials are graphitic in nature. The I_D/I_G ratio varies between 1.94 (CQD-neg), 1.56 (CQD-pos), and 1.32 (CQD-neut), suggesting their large surface disorder and amorphous nature (Table 1).

Before investigating in more detail the possibility of these nanostructures to inhibit hIAPP aggregation, the cytotoxic effects of CQD-pos, CQD-neut and CQD-neg were measured by the resazurin assay. Fig. 7 shows no cytotoxic effects of the CQDs at a concentration of 1–100 μg mL^{-1} on rat insulinoma cells (Fig. 7a) and primary isolated rat islets (Fig. 7b).

To understand the aggregation inhibition potential of CQDs on hIAPP, 20 μM hIAPP was incubated with 10 and 100 μg mL^{-1} CQD-pos first in the presence or absence of glucose or palmitate. In the absence of glucose and palmitate, we found that 10 μg mL^{-1} CQD-pos slowed and reduced the

Table 1 Physicochemical properties of the three CQDs

Particle	Hydrodynamic size/nm	ζ/mV	TEM/nm	O $_{1s}$ (at%)	N $_{1s}$ (at%)	F $_{1s}$ (at%)
CQD-pos	10.6 ± 2.3 (63%) 265 ± 199 (37%)	+32.5 ± 0.8	16.8 ± 6.7	14.4	13.7	—
CQD-neut	225 ± 199 (84%) 42±9 (16 %)	−0.4 ± 0.6	22.3 ± 5.7	12.6	—	3.9
CQD-neg	389 ± 123 (100%)	−24.0 ± 1.6	20.8 ± 6.6	22.8	5.7	—

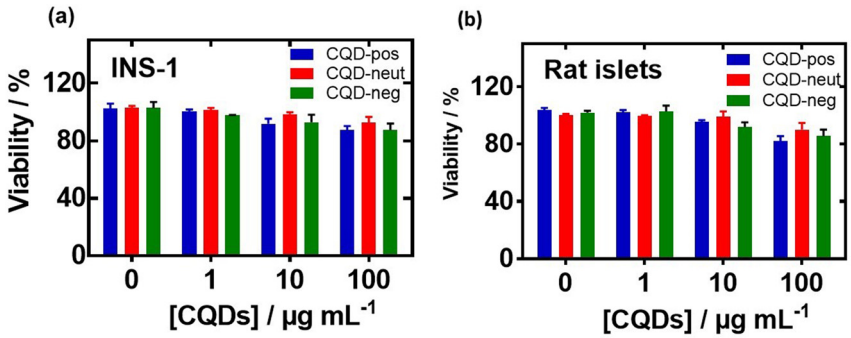

Fig. 7 Cell viability of rat insulinoma cell (INS-1) and primary isolated rat islets in the presence of carbon quantum dots: CQD-pos (red), CQD-neut (green) and CQD-neg (blue) at different concentrations (1, 10 and 100 μg mL^{-1}) applied to the cells and incubated for 24 h. Negative control: without CQDs. (a) Rat insulinoma cell line (INS-1) and (b) primary isolated rat islets: the cells were cultured in RPMI-1640 medium supplemented with 10% fetal bovine serum (FBS), 1% penicillin–streptomycin, 1% sodium pyruvate, and 50 μM β-mercaptoethanol. They were seeded at a density of 10^5 cells per well in a 96-well plate and grown for 24 h before the assay. The cell viability was evaluated using the resazurin cell viability assay. The results are expressed as the mean ± SEM of at least 3 independent samples for each group. Using a two-way ANOVA test, all data were statistically n.s. when compared to the control (0 μg mL^{-1}).

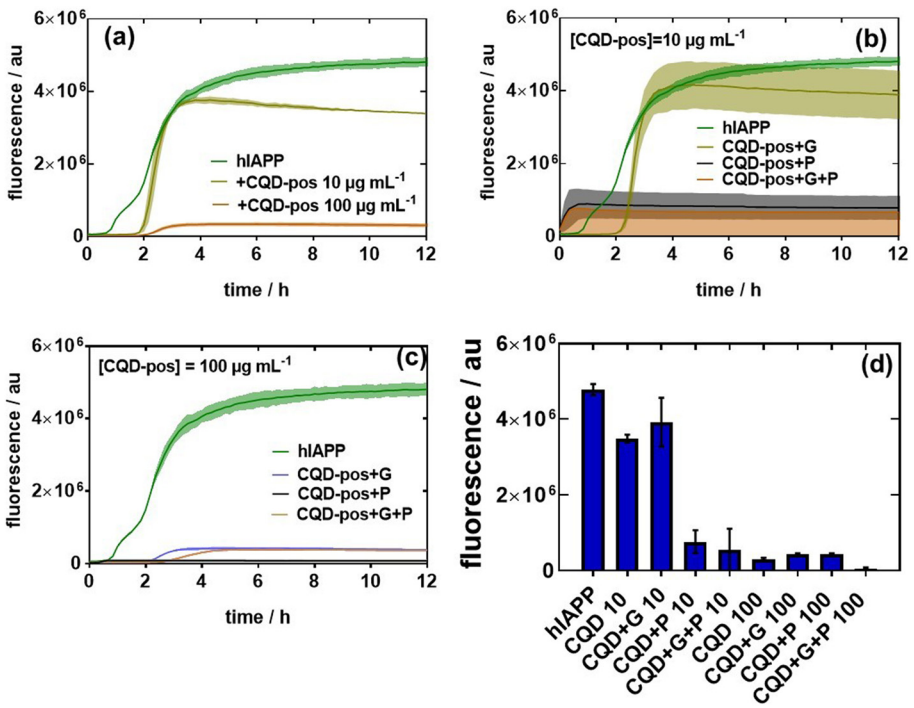

Fig. 8 Influence of CQD-pos on hIAPP fibrillation in the absence and presence of glucose and palmitate: (a) fluorescence assays based on ThT fluorescence in the presence of hIAPP (20 μM) and the effect of different concentrations (10 and 100 μg mL^{-1}) of CQD-pos on hIAPP aggregation. (b) Effect of glucose (G, 11 mM) and palmitate (P, 500 μM) and a mixture of both on hIAPP fibrillation (20 μM) in the presence of 10 μg mL^{-1} CQD-pos. (c) Same as (b) but in the presence of 100 μg mL^{-1} CQD-pos. (d) Comparison of ThT fluorescence intensities after 12 h for hIAPP (control) and in the presence of glucose, palmitate and CQD-pos. The results are expressed as the mean ± SEM of at least 3 independent samples for each group.

amplitude of hIAPP fibrillation (Fig. 8a). The effect of CQD-pos was more pronounced at 100 μg mL^{-1}. Indeed, the fluorescence intensity after 12 h is significantly lower (almost marginal signal) than that of 10 μg mL^{-1} CQD-pos. How the diabetogenic environment influences the behavior and the effect of the presence of 10 and 100 μg mL^{-1} CQD-pos on hIAPP aggregation is described in Fig. 8b and c. The overall inhibitory effect of CQD-pos on hIAPP fibrillation was maintained at

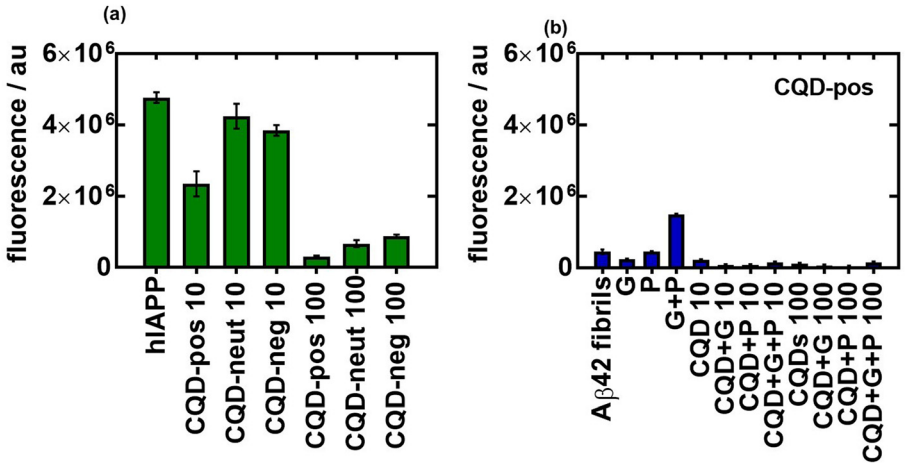

Fig. 9 Influence of the charge of CQDs on hIAPP and Aβ42 aggregation: (a) comparison of ThT fluorescence intensities after 12 h for hIAPP (control) and in the presence of glucose (G, 11 mM), palmitate (P, 0.5 mM) and CQDs of different charges at 10 and 100 μg mL^{-1}. (b) Comparison of the ThT fluorescence intensities after 12 h for Aβ42 (control) and in the presence of glucose (G, 11 mM), palmitate (P, 0.5 mM) and CQDs-pos at 10 and 100 μg mL^{-1}. The results are expressed as the mean ± SEM of at least 3 independent samples for each group.

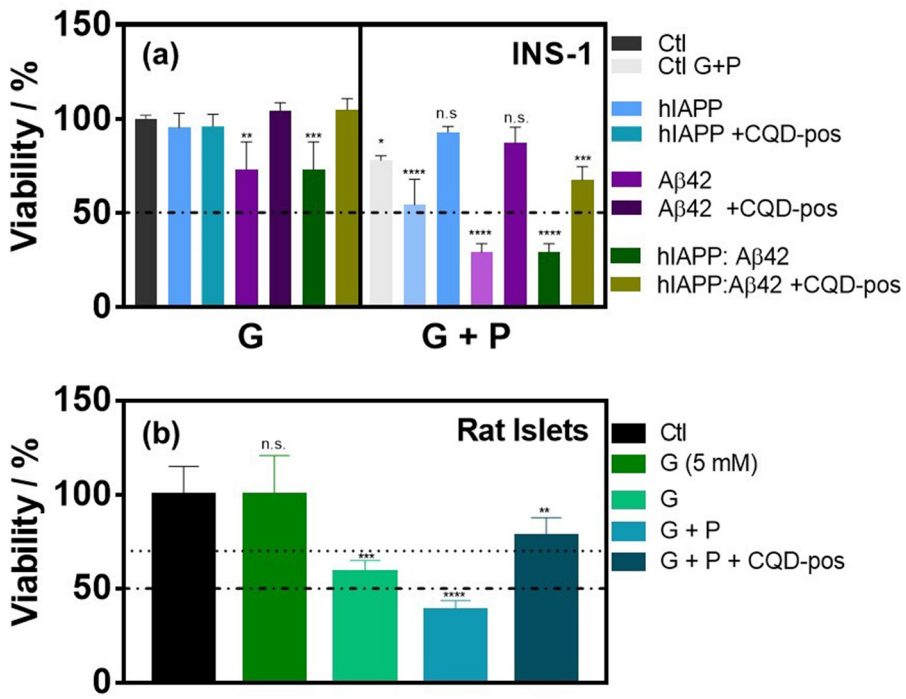

Fig. 10 Viability of INS-1 cell and primary isolated rat islets exposed to CQD-pos. (a) Viability of INS-1 cells cultured in a medium supplemented with 0.1% (vol/vol) of BSA and containing 11 mM glucose (G) or 11 mM glucose and 0.5 mM palmitate (G + P) in the absence (Ctl, black) or presence of aggregated (6 h, 37 °C) hIAPP (20 μM), Aβ42 (20 μM) and hIAPP:Aβ42 mixtures (1 : 1) only or in the presence of 100 μg mL^{-1} CQDs-pos. The results are expressed as the mean ± SEM of at least 3 independent samples for each group. $p > 0.05$ (n.s.); *$p < 0.05$; **$p < 0.01$; ***$p < 0.001$; and ****$p < 0.0001$, a one-way ANOVA test against control. (b) Viability of primary isolated rat islets exposed for 72 h to aggregated (6 h, 37 °C) 20 μM hIAPP:Aβ42 mixture (1 : 1) under non-diabetic conditions (G = 5 mM), diabetic conditions (G = 11 mM) and in the presence of 11 mM glucose and 0.5 mM palmitate (G + P) with or without 100 μg mL^{-1} CQDs-pos.

high glucose (11 mM) and palmitate (0.5 mM) concentrations (Fig. 8b). In the presence of glucose, inhibition of hIAPP with 10 μg mL^{-1} CQD-pos is somehow less efficient as a higher mean fluorescence signal is observed, as shown in Fig. 8b. Palmitate alone and palmitate together with glucose show an increase in fluorescence in the first 1 h and then stabilization to a comparable level than under control conditions. In the case of 100 μg mL^{-1} CQD-pos, no aggregation was observed in the presence of glucose and palmitate (Fig. 8c). Indeed, comparing the fluorescence intensity of the different tests (Fig. 8d), 100 μg mL^{-1} CQD-pos seem to effectively inhibit hIAPP aggregation. Most importantly, the inhibition effect of 100 μg mL^{-1} CQD-pos on hIAPP in the presence of glucose (11 mM) and palmitate (500 μM) when incubated in cell culture medium supplemented with 0.1% (vol/vol) of BSA, as used later for estimating the viability of INS-1 cells and primary isolated rat islets, shows the same behavior as outlined in Fig. 8c. Even though a protein corona will be present on the CQDs-pos, no special treatment seems to be required to maintain the approach in *in vitro* and *ex vivo* tests.

The effect of charge on the aggregation behavior of hIAPP, in the presence and absence of glucose and palmitate, was determined by comparing the results of CQD-pos with the other two CQDs *i.e.* CQD-neut and CQD-neg (Fig. 9a). At lower (10 μg mL^{-1}) and high concentrations (100 μg mL^{-1}), the charge effect seems to be in favor of CQD-pos. hIAPP carries a net charge of +36.8 mV at neutral pH. The inhibitory effect occurs thus most likely through electrostatic repulsion between CQD-pos and hIAPP. A similar effect was reported with PEI-modified Ag NPs with a zeta potential of +40.0 mV.[29] CQD-pos were used in the following experiments to further understand Aβ42 aggregation in the presence and absence of glucose and palmitate (Fig. 9b). In line with the difference in their structure and conformation, we found Aβ42 and hIAPP aggregation to be different. Indeed, the fluorescence intensity of Aβ42 reached after 12 h is low (Fig. 9b) compared to that of hIAPP (Fig. 1a). Th presence of CQD-pos even at only 10 μg mL^{-1} interfered strongly with aggregation with an almost zero fluorescence signal.

When added to INS-1 cells, we found that single oligomers are toxic for β-cells in the presence of glucose and palmitate. The cytotoxicity was more prominent for the Aβ42 oligomers and the heteromeric hIAPP:Aβ42 complex when compared to hIAPP alone under diabetic conditions and in the presence of palmitate. When Aβ42 and the heteromer hIAPP:Aβ42 aggregations were inhibited by CQD-pos, the toxicity was efficiently alleviated (Fig. 10a), being statistically comparable in the case of Aβ42 to the control. It is important that no other modifications are necessary to maintain the effectiveness of the nanoparticles *in vitro*. This result was confirmed using primary isolated rat islets. Indeed, the hIAPP:Aβ42 oligomer exacerbated the cytotoxicity of the diabetogenic environment, including glucose and palmitate, and the prevention of hIAPP:Aβ42 aggregation by CQD-pos alleviated the cytotoxicity of the medium (Fig. 10b).

3. Conclusion

The results of this study provide evidence that glucose and palmitate as SFA play a key role in the amyloidogenesis of hIAPP and Aβ42. Palmitate was of high importance for increased hIAPP aggregation over a time span of 24 h. Most important is that our findings confirm that heteromerization of Aβ42 and hIAPP can be accelerated by a diabetogenic environment. In addition, the hIAPP:Aβ42 heterocomplex was clearly found to be more cytotoxic than single oligomers and/or aggregates of hIAPP in INS-1 rat cells. Our findings unveil the critical role of the Aβ42 oligomers/aggregates in the cytotoxicity caused by the heterocomplex. In the presence of high glucose concentration and palmitate, the Aβ42 oligomers/aggregates *per se* are sufficient for reducing the cell viability. These results support the hypothesis that Aβ42 oligomers/aggregates are a critical component within the amyloid deposit found in the islets of patients with T2D, which form a harmful heteromeric complex with hIAPP in the pancreatic β-cells exposed to chronic hyperglycemia and SFAs. Finally, positively charged carbon quantum dots (CQD-pos) *in vitro* proved to be efficient in inhibiting the cytotoxic effect of the hIAPP:Aβ42 heterocomplex in β-cells under the diabetogenic environment. CQD-pos significantly altered both the fibrillation rate and the physical properties of hIAPP at a concentration of 100 μg mL^{-1}, likely mediated by electrostatic repulsion. Some studies have shown that up to 400 μg mL^{-1} CQDs are not toxic in mice.[30] This suggests that 100 μg mL^{-1} CQDs can be used for preclinical studies investigating the safety and efficiency of CQD-pos in reducing fibrillation and islet amyloid deposit formation in animal models of T2D. Such pre-clinical experiments are keys to validate the realistic use of CQD-pos for clinical purposes. While the effects of a number of nanostructures on hIAPP fibrillation and the mesoscopic properties of hIAPP have been explored and discussed in the literature, none of these studies were performed under real T2D conditions.

Our work underlines that nanomaterials in the form of CQD-pos are efficient in the inhibition of protein fibrillation under diabetic conditions and pave the way for developing innovative nanoparticle-based strategies to prevent β-cell death in T2D.

4. Experimental section

4.1. Materials

The human amylin [8–37] peptide (hIAPP, ref. 350044) and human beta-amyloid [1–42] (Aβ42, ref. AS-20276) were purchased from Cliniscience (France) and Eurogentech (USA), respectively. Dulbecco's modified Eagle's medium (DMEM, ref. L0101-500) was obtained from Ozyme (France). Fetal calf serum (FCS, ref. CVFSVF00-01*) and 10× Tris/glycerine/SDS buffer (ref. 5460-0016) were obtained from Eurobio Scientific (France). Phosphate-buffered saline (PBS 1×, pH 7.4, Gibco®, ref. 11503387), penicillin–streptomycin (Gibco®, ref. 15140122), RPMI 1640 medium (ref. 12027599), Williams E

medium (ref. 22551022), sodium pyruvate (Gibco®, ref. 11530396), β-mercaptoethanol (Gibco®, ref. 11528926), PrestoBlue™ HS cell viability reagent (ref. 16294822), dimethyl sulfoxide (DMSO, ref. 10206581), hydrofluoric acid (HF, ref. 10418600), polyclonal antibody (ref. 10717433), anti-rabbit HRP secondary antibody (ref. 11859140) and pre-wetted dialysis membranes (SpectraPor RC, 1 kDa, ref. 11540980) were obtained from Fisher-Scientific (France). Glucosamine hydrochloride (ref. G4875), ethylenediamine (ref. 03550), β-alanine (ref. 146064), sodium hydroxide (NaOH, ref. 30620), dexamethasone (ref. D0700000), sodium palmitate (ref. P9767), thioflavin T (ThT, ref. T3516), 1,1,1,3,3,3-hexafluoro-2-propanol (HFIP, ref. 8.45157), glucose (ref. 158968), Ponceau S solution (ref. P7170) and bovine serum albumin (BSA, ref. A4503) were purchased from Merck (France). Clarity Western Peroxide Reagent, Clarity Western Luminol/Enhancer Reagent (ref. 1705061), Mini PROTEAN TGX Stain-Free precast gels for polyacrylamide gel electrophoresis (ref. 4561084) and nitrocellulose membranes (ref. 1704158) were purchased from Bio-Rad, France. The ASTM type I ultrapure water (resistivity = 18.2 MΩ cm) used for all the experiments was purified with an Arium® Comfort I water purification system (Sartorius).

4.2. Synthesis of carbon quantum dots (CQDs)

CQD-pos were prepared in a 30 mL G30 vial from a solution of glucosamine hydrochloride (1.00 g, 4.63 mmol) in distilled water (20 mL) and ethylenediamine (0.307 g, 1.1 eq.) under stirring to ensure homogeneity. The reactor was then placed in a microwave reactor (Monowave 450, Anton-Parr). The solution was heated under pressure for 5 min from room temperature to 200 °C and then maintained for 10 min at 200 °C under stirring (1200 rpm). The resulting brown solution was centrifuged at +4 °C (10 000*g*, 10 min) in order to remove big particles. The supernatant was dialyzed against water for 24 h (SpectraPor RC membranes, 1 kDa) and then kept (or lyophilized) to yield a brown solution.

CQD-neut was synthesized according to a procedure described previously.[31] Briefly, 4 mL of an aqueous solution of hydrofluoric acid (HF) was mixed with 10 mL of 1% glucose aqueous solution in a 30 mL SiC vessel vial C30 Wide Neck. The mixture was placed in a microwave reactor (Monowave 450, Anton-Parr) and kept under continuous stirring at 180 °C for 1 h until a brown color dispersion was produced. In order to remove larger particles, the dispersion was filtered through a 0.2 μm filter and the pH was neutralized with 1 M NaOH. The supernatant was dialyzed against water for 24 h (SpectraPor RC membranes, 1 kDa) and then kept undisturbed (or lyophilized) to yield a brown solution.

CQD-neg was synthesized according to a modified procedure.[32] To a stirring solution of glucosamine hydrochloride (1.00 g, 4.63 mmol) in distilled water (20 mL) in a 30 mL G30 vial, β-alanine (0.454 g, 1.1 eq.) was added and stirred to ensure homogeneity. The reactor was then placed in a microwave reactor (Monowave 450, Anton-Parr). The solution was heated under pressure for 2 min from room temperature to 200 °C and then maintained for 1 min at 200 °C under stirring (1200 rpm). The resulting brown solution was centrifuged at 4 °C (10 000*g*, 10 min) in order to remove the big particles. The supernatant was dialyzed against water for 24 h (SpectraPor RC membranes, 1 kDa) and then kept (or lyophilized) to yield a brown solution.

4.3. Characterization and instrumentation

Transmission electron microscopy (TEM). The morphology and size of the CQDs were characterized using an FEI Tecnai G2-20 microscope.

Fourier transform infrared (FT-IR) spectroscopy. FT-IR analyses were performed using a Thermo Fisher Scientific Inc. Nicolet 8700 in the frequency range of 650 and 4000 cm^{-1} with a resolution of 6 cm^{-1}. Dried CQDs (around 1 mg) were mixed with potassium bromide powder (200 mg) in an agar mortar. The mixture was pressed into a pellet under 7 tons of load for 10 min and the spectrum was recorded immediately. An average of 64 scans was recorded for each sample.

X-ray photoelectron spectroscopy (XPS). The XPS spectra were recorded using a VG Escalab 220XL spectrometer from Vacuum Generators featuring a monochromatic Al Kα X-ray source (1486.6 eV) and a spherical energy analyzer operated in the CAE (constant analyzer energy) mode (CAE = 100 eV for survey spectra and CAE = 40 eV for high-resolution spectra), using the electromagnetic lens mode. The angle between the incident X-rays and the analyzer is 58° and the detection angle of the photoelectrons is 30°.

DLS measurements. The average hydrodynamic diameter and the zeta-potential were recorded using a Zetasizer® Nano ZS (Malvern Instruments S.A., Worcestershire, UK). All the batches were diluted to 200 μg mL^{-1} in ultrapure water and analyzed in triplicate at 20 °C. The zeta potential of CQDs in ultrapure water (200 μg mL^{-1}) was measured at 20 °C using a folded zeta capillary cell (DTS1070). The experiments consisted of 15 runs per measurement with an applied voltage of 150 V.

Raman spectroscopy. Raman spectroscopy measurements were performed using a LabRam HR Micro-Raman system (Horiba Jobin Yvon) using a 473 nm laser diode as the excitation source. CQDs were deposited on a clean silicon wafer. The visible light is focused using a 100× objective. The scattered light is collected from 100 to 4000 cm^{-1} by the same objective in the backscattering configuration, dispersed by a 1800 mm focal length monochromator and detected using a CCD camera.

4.4. Biological assays

Cytotoxicity tests of CQDs. The cytotoxicity of the prepared CQDs was tested at concentrations of 1, 10 and 100 μg mL^{-1}. The rat insulinoma cell line (INS-1) was routinely cultured in RPMI-1640 medium supplemented with 10% fetal bovine serum (FBS, Gibco®), 1% penicillin–streptomycin (Gibco®), 1% sodium pyruvate, and 50 μM β-mercaptoethanol. For the cytotoxicity experiments, the cells were seeded at a density of 10^5 cells per well in a 96-well plate and grown for 24 h before assay. The culture medium was replaced with a FBS-free fresh medium that contains CQDs at 1, 10 and 100 μg mL^{-1}. After

24 h, the medium was aspirated and the cells were washed with PBS. The cell viability was evaluated using resazurin cell viability. Briefly, the PrestoBlue™ viability reagent diluted in complete medium (1 : 10) was added to each well and the plate was incubated for 1 h in a humidified incubator. The fluorescence emission of each well was measured at 593 nm (20 nm bandwidth) with excitation at 554 nm (18 nm bandwidth) using a Cytation™ 5 Cell Imaging Multi-Mode Reader (BioTek Instruments SAS, France). The fluorescence of cells was normalized by subtracting this from the culture medium without cells in which the reagent was included. Each condition was replicated three times and the mean fluorescence value of non-exposed cells was taken as 100% cellular viability.

Thioflavin T kinetics assay. To assess the fibrillization kinetics of hIAPP and Aβ42 in the presence of CQDs, a freshly prepared 573.8 μM ThT solution was mixed with samples in a 1 : 2 molar ratio of ThT:peptide. The final concentration of hIAPP was 20 μM. The assays were performed at 37 °C on a Nunc™ MicroWell™ white polystyrene 96-well plate and the changes in ThT fluorescence were recorded every 10 min over 15–25 h at an excitation/emission wavelength of 440/484 nm using a Cytation™ 5 multi-mode microplate reader. All samples were analyzed in triplicate.

Preparation of peptides and heterocomplexes. Dry peptides were weighed and dissolved in 1,1,1,3,3,3-hexafluoro-2-propanol (HFIP) for 1 h at room temperature (RT) and then separated into 100 μg aliquots. The HFIP was allowed to evaporate overnight at RT, producing dry peptide films that were stored at −20 °C for future use. Before each experiment, fresh Aβ42 and hIAPP solutions were prepared by initially solubilising the dry peptide in dimethyl sulfoxide (DMSO, Thermo Fisher) to make a 2.5 mM stock. Aβ42 and hIAPP were mixed in a ratio of 1 : 1 to obtain a final concentration of 20 μM. The peptide solutions were incubated at 4 °C and 37 °C for 24 h to allow the formation of oligomers and fibrils, respectively.

Western blotting of hIAPP:Aβ42 aggregates. To perform western blotting, first, the proteins were denatured for 3 min at 95 °C. For gel electrophoresis, 50 μg of total denatured proteins was separated in precast 4–15% TGX stain free gels at 200 V in 30 min. Subsequently, the gels were blotted to nitrocellulose membranes at 250 mA for 2 h. Immunoblotting of aggregates was performed using β-amyloid (1–42) rabbit specific primary antibody and anti-rabbit HRP secondary antibody. Analysis of the western blot was performed using Clarity ECL substrates based on the chemiluminescent revelation process. The imaging of the membrane was performed using a ChemiDoc MP Imaging System. ImageJ was used for quantification.

Preparation of palmitate. A solution of the saturated fatty acid (SFA) palmitate (100 mM) was prepared by dissolving it in 0.1 N NaOH at 70 °C. Subsequently, this solution was diluted in a ratio of 1 : 10 in 10% (w/v) bovine serum albumin (BSA) and incubated at 55 °C for 10 min to achieve a stock solution of 10 mM palmitate.

Cytotoxicity tests of hIAPP, Aβ42 and hIAPP aggregates as well as hIAPP:Aβ42 heterocomplexes under diabetogenic conditions. To test the cytotoxic effect of hIAPP, Aβ42 and hIAPP:Aβ42 heterocomplexes, INS-1 cells were seeded at a density of 5×10^5 cells per well in a 96-well plate and grown for 24 h before assay, as described above. The culture medium was replaced with fresh glucose- and FBS-free medium containing 0.5 mM of palmitate, 11 mM of glucose or 10% of BSA and 11 mM of glucose (control experiment). The aggregates at the concentrations of 20 μM for hIAPP and Aβ42 and 2/20 μM for hIAPP:Aβ42 heterocomplexes were added and incubated for 48 h at 37 °C. The cell viability was evaluated using the resazurin cell viability assay as described above.

Cytotoxicity tests of CQDs in isolated rat islets. Rat islets were isolated from the pancreas of Sprague-Dawley rats by ductal injection of collagenase. The purification and culture of islets were conducted as described in ref. 33. Islets (40 per well/condition) were handpicked and placed on inserts within 24-well plates 24 h before the assay. Placing islets on the inserts preserves the number and quality of islets during the medium changes. The culture medium containing serum was replaced by the culture medium containing different CQDs with concentrations of 1, 10 and 100 μg mL^{-1}. The cell viability was evaluated after 24 h of incubation using the resazurin cell viability assay, as described above.

Cytotoxicity tests of aggregated hIAPP:Aβ42 heterocomplexes in isolated rat islets exposed to diabetogenic conditions. To measure the cytotoxicity of hIAPP:Aβ42 heterocomplexes under diabetogenic conditions, we used 40 handpicked isolated rat islets. The islets were cultured for 72 h at 37 °C in a glucose-free medium supplemented with 10% fetal bovine serum (FBS, Gibco®) and 1% penicillin–streptomycin (Gibco®), containing either 0.5 mM of palmitate, 11 mM of glucose or 10% of BSA and 11 mM of glucose (control experiment). In this medium, we added 20 μM aggregates for hIAPP:Aβ42 heterocomplexes. The medium replacement was achieved by moving up the islet-containing inserts. The cell viability was evaluated using the resazurin cell viability assay as described above.

Animal procedures were performed in accordance with the Guidelines for Care and Use of Laboratory Animals of CHU Lille and the experiments were approved by the Animal Ethics Committee of CHU Lille.

Conflicts of interest

There are no conflicts to declare.

Acknowledgements

AV thanks the I-SITE University of Lille Foundation for a PhD fellowship. Financial support from the CNRS and ULille is acknowledged. This work was partly supported by the French Renatech network.

References

1 A. Clark, M. F. Saad, T. Nezzer, C. Uren, W. C. Knowler, P. H. BEnnett and R. C. Turner, *Diabetologia*, 1990, **33**, 285–289.

2 J. C. Ehrlich and I. M. Ratner, *Am. J. Pathol.*, 1961, **38**, 49–59.

3 C. A. Jurgens, M. N. Toukatly, C. L. Fligner, J. Udayasankar, S. L. Subramanian, S. Zraika, K. Aston-Mourney, D. B. Carr, P. Westermark, G. T. Westermark, S. E. Kahn and L. L. Hull, *Am. J. Pathol.*, 2011, **178**, 2632–2640.

4 P. Westermark, A. Andersson and G. T. Westermark, *Physiol. Rev.*, 2011, **91**, 795–826.

5 G. Forloni and C. Balducci, *J. Alzheimer's Dis.*, 2018, **62**, 1261–1276.

6 R. Ehehalt, B. Michel, D. De Pietri Tonelli, D. Zacchetti, K. Simons and P. Keller, *Biochem. Biophys. Res. Commun.*, 2002, **293**, 30–37.

7 D. J. Figueroa, X. P. Shi, S. J. Gardell and C. P. Austin, *J. Alzheimer's Dis.*, 2001, **3**, 393–396.

8 G. Finzi, F. Franzi, C. Placidi, F. Acquati, E. Palumbo, A. Russo, R. Taramelli, F. Sessa and S. La Rosa, *Ultrastruct. Pathol.*, 2008, **32**, 6.

9 J. Miklossy, H. Qing, A. Radenovic, A. Kis, B. Vileno, F. Laszlo, L. Miller, R. N. Martins, G. Waeber, V. Mooser, F. Bosman, K. Khalili, N. Darbinian and P. L. McGeer, *Neurobiol. Aging*, 2010, **31**, 1503–1515.

10 P. Bharadwaj, T. Solomon, B. R. Sahoo, K. Ignasiak, S. Gaskin, J. Rowles, G. Verdile, M. J. Howard, C. S. Bond, A. Ramamoorthy, R. N. Martins and P. Newsholme, *Sci. Rep.*, 2020, **10**, 10356.

11 J. A. Kulas, K. L. Puig and C. K. Combs, *J. Endocrinol.*, 2017, **235**, 49–67.

12 M. E. Oskarsson, J. F. Paulsson, S. W. Schultz, M. Ingelsson, P. Westermark and G. T. Westermark, *Am. J. Pathol.*, 2015, **185**, 834–846.

13 Z. Tu, M. P. Keller, C. Zhang, M. E. Rabaglia, D. M. Greenawalt, X. Yang, I. M. Wang, H. Dai, M. D. Bruss, P. Y. Lum, Y.-P. Zhou, D. M. Kemp, C. Kendziorski, B. S. Yandell, A. D. Attie, E. E. Schadt and J. Zhu, *PLoS Genet.*, 2012, **8**, e1003107.

14 P. C. Ken, M.-A. Sani, F. Ding, A. Kakinen, I. Javed, F. Separovic, T. P. Davis and R. Mezznga, *Chem. Soc. Rev.*, 2017, **46**, 6492.

15 K. Koppel, H. Tang, I. Javed, M. Parsa, M. Mortimer, T. P. Davis, S. Lin, A. L. Chaffee, F. Ding and P. C. Keg, *Nanoscale*, 2020, **12**, 12317–12328.

16 G. Wei, Z. Su, N. P. Reynolds, P. Arosio, I. W. JHamley, E. Gazitf and R. Messenga, *Chem. Soc. Rev.*, 2017, **46**, 4661.

17 I. Javed, G. Peng, Y. Xing, T. Yu, M. Zhao, A. Kakinen, C. L. Parish, F. Ding, T. P. Davis, P. C. Ke and S. Lin, *Nat. Commun.*, 2019, **10**, 3780.

18 M. Wang, Y. Sun, X. Cao, G. Peng, I. Javed, A. Kakinen, T. P. Davis, S. Lin, J. Liu, F. Ding and P. C. Ke, *Nansocale*, 2018, **10**, 19995–20006.

19 M. Yousaf, H. Huang, C. Wang and Y. Yang, *ACS Chem. Neurosci.*, 2017, **8**, 1368–1377.

20 Y. Zhou, P. Y. Liyanage, D. Devadoss, L. R. R. Guevara, L. Ling Cheng, R. M. Graham, H. S. Chand, A. O. Al-Youbi, A. S. Bashammakh, M. S. El-Shahawi and R. M. Leblanc, *Nanoscale*, 2019, **11**, 22387.

21 K. Ono, R. Takahashi, T. Ikeda, M. Mizuguchi, T. Hamaguchi and M. Yamada, *Biochim. Biophys. Acta*, 2014, **1842**, 646–653.

22 A. Mukherjee, D. Morales-Scheihing, N. Salvadores, I. Moreno-Gonzalez, C. Gonzalez, K. Taylor-Presse, N. Mendez, M. Shahnawaz, A. O. Gaber, O. M. Sabek, D. W. Fraga and C. Soto, *J. Exp. Med.*, 2017, **214**, 2591–2610.

23 Z. Ma and G. T. Westermark, *Mol. Med.*, 2002, **8**, 863–868.

24 X.-D. Mo, L.-P. Gao, Q.-J. Wang, J. Yin and J. Y.-H. Jing, *Lipids Health Dis.*, 2018, **17**, 42.

25 E. Karaskov, C. Scott, L. Zhang, T. Teodoro, M. Ravazzola and A. Volchuk, *Endocrinology*, 2006, **147**, 3398–3407.

26 D. A. Cunha, P. Hekerman, L. Ladrière, A. Bazarra-Castro, F. Ortis, M. C. Wakeham, F. Moore, J. Rasschaert, A. K. Cardozo, E. Bellomo, L. Overbergh, C. Mathieu, R. Lupi, T. Hai, A. Herchuelz, P. Marchetti, G. A. Rutter, D. L. Eizirik and M. Cnop, *J. Cell Sci.*, 2008, **121**, 2308–2318.

27 A. Barras, F. Sauvage, I. de Hoon, K. Braeckmans, D. Hua, G. Buvat, J. C. Fraire, C. Lethien, J. Sabag, M. Harrinton, A. Abderrahmani, R. Boukherroub, S. de Smedt and S. Szunerits, *Nanoscale Horiz.*, 2021, **6**, 449–461.

28 L. Liu, M. Zhang, Z. Xiong, D. Hu, G. Wu and P. Chen, *Carbon*, 2015, **81**, 702–709.

29 M. Wang, A. Kakinen, E. H. Pilkington, T. P. Davis and P. C. Ke, *Biomater. Sci.*, 2017, **5**, 485.

30 S.-T. Yang, L. Cao, P. G. Luo, F. Lu, X. Wang, H. Wang, M. J. Meziani, Y. Liu, G. Qi and Y.-P. Sun, *J. Am. Chem. Soc.*, 2009, **131**, 11308–11309.

31 M. Yousaf, H. Huang, P. Li, C. Wang and Y. Yang, *ACS Chem. Neurosci.*, 2017, **8**, 1368–1377.

32 S. A. Hill, D. Benito-Alifonso, S. A. Davis, D. J. Morgan, M. Berry and M. C. Galan, *Sci. Rep.*, 2018, **8**, 12234.

33 A. Abderrahmani, G. Niederhauser, D. Favre, S. Abdelli, M. Ferdaoussi, J. Y. Yang, R. Regazzi, C. Widmann and G. Waeber, *Diabetologia*, 2007, **50**, 1304–1314.